BEARINGLESS SINGLE-PHASE MOTOR WITH CONCENTRATED FULL PITCH WINDINGS IN INTERIOR ROTOR DESIGN

Wolfgang Amrhein,[1] Siegfried Silber[2]

ABSTRACT

Bearingless motors are commonly used in special applications with high demands on speed range, lifetime, cleanness or tightness. The integration of distributed 3-phase motor windings and 3-phase radial magnetic bearing windings with sinusoidal current density distribution leads to a high number of stator coils and high manufacturing costs in comparison with ordinary ball bearing motors.

For this reason a new bearingless low cost motor has been developed. It is a single-phase motor with only four concentrated full pitch coils for controlling both torque and levitation. The speed and position control is performed by superposition of lateral force and radial force current components in the windings. Owing to the nonsinusoidal stator current density distribution the Maxwell and Lorentz force vectors move on elliptical locus curves when the permanent magnet rotor is rotated at constant current. Thus special transformation functions have to be used for control of rotor position. The stabilization of the rotor disc position in axial and tilting direction is passively achieved by the magnetic tensible force, supported by suitably selected diameter / axial length ratio of the magnetic components.

Possible applications of the bearingless single phase motor are electrical machines with low starting torque like fluid pumps, vacuum pumps, fans or blowers.

INTRODUCTION

Generally magnetic bearing drive systems are only used in special applications, where roller or sliding bearings cannot serve high demands on speed range, lifetime, cleanness or tightness. A conventional magnetic bearing drive system usually consists of a three-phase motor, two four-phase radial magnetic bearings, one two-phase axial magnetic bearing, two auxiliary roller bearings and thirteen power converter units in all. Therefore the mechanical and electronical expenditure is very high.

[1]Johannes Kepler University, Dept. of Power Electronics and Electrical Drives, Altenberger Str. 69, A-4040 Linz, Austria, e-mail: amrhein@mechatronik.uni-linz.ac.at, tel.: +43 732 2468 9715, fax: +43 732 2468 9719.
[2]Johannes Kepler University, Dept. of Power Electronics and Electrical Drives, Altenberger Str. 69, A-4040 Linz, Austria, e-mail: silber@mechatronik.uni-linz.ac.at, tel.: +43 732 2468 9720.

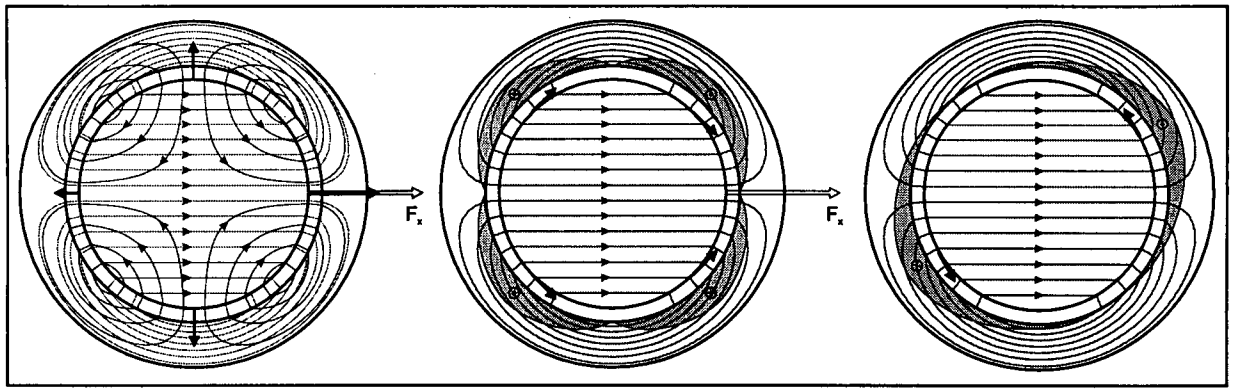

Fig. 1a: Maxwell forces for a pole pair combination p_R=1, p_{S1}=2.

Fig. 1b: Lorentz forces for a pole pair combination p_R=1, p_{S1}=2.

Fig. 1c: Torque generation by Lorentz forces for a pole pair combination p_R=1, p_{S2}=1.

In the last ten years new constructions of bearingless drive systems have been presented in which the motor and the magnetic bearing winding systems are integrated in the same stator core as shown in figure 1 (Bichsel, 1990; Schöb, 1993; Schöb and Bichsel, 1994; Ohishi et al., 1994; Bleuler et al., 1994; Chiba and Fukao, 1994; Schöb and Barletta, 1996; Oshima et al., 1996). In figure 1 the radial force and torque production of a bearingless motor is explained in principle. For separate control of radial forces and lateral forces (torque) the pole pair numbers of the three-phase magnetic bearing winding (p_{S1}=2) and the three-phase motor winding (p_{S2}=1) must differ by one. To get sinusoidal current density distributions the stator coils are distributed in several slots and fractional pitch windings are used as well. It is assumed that the flux distribution of the rotor (p_R=1) is sinusoidal. By the interaction of the four-pole stator winding and the two-pole rotor field Maxwell and Lorentz forces are produced. Figure 1a shows the Maxwell forces (reluctance forces) created by the superposition of the rotor and armature fields in the air gap. In figure 1b the corresponding Lorentz forces (forces on conductors) are presented. Amplitude and angle of the resulting force vector are controlled by the stator current space vector of the four-pole winding (Schöb and Bichsel, 1994). For the reason of different pole pair numbers of the rotor field and armature winding there is no torque production in figure 1a and 1b. The torque has to be controlled using a separate winding with a pole pair number equal to that of the rotor (figure 1c).

For applications like pumps or blowers, which don't need a very stiff stabilization in axial and tilting direction, figure 2 shows a constructional principle of bearingless motors with only 2+1 controlled degrees of freedom (x-, y- coordinates of the rotor plane, rotation angle δ). The stabilization of the rotor disc position in axial and tilting direction is passively achieved by the tensible force of the permanent magnet, supported by suitably selected diameter/axial-length ratio of the magnetic components (Schöb and Barletta, 1996; Bleuler et al., 1994).

DESIGN OF THE BEARINGLESS MOTOR

In the following discussion a new development of a bearingless permanent magnet motor is presented. In contrast to previous proposals the magnetic bearing is integrated into a single-phase motor using concentrated full-pitch coils. The bearingless single-phase motor shown in

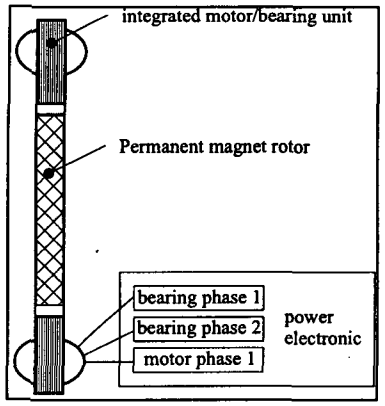

Fig. 2: Integrated motor/magnetic bearing unit with only 2+1 controlled degrees of freedom.

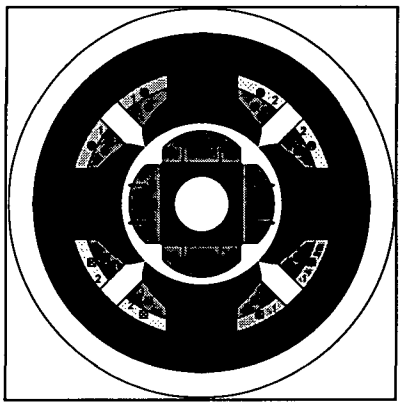

Fig. 3: Bearingless motor design with only three phases.

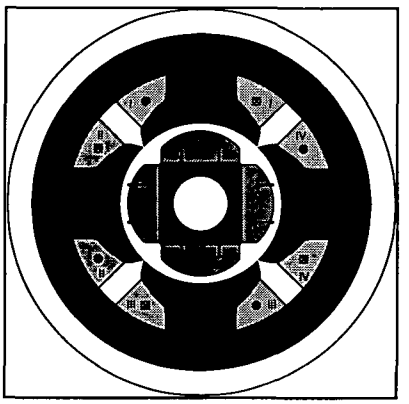

$i_I=i_1-i_2+i_3$; $i_{II}=-i_1-i_2-i_3$; $i_{III}=-i_1+i_2+i_3$; $i_{IV}=i_1+i_2-i_3$.

Fig. 4: Bearingless four-phase motor design with only four concentrated full pitch coils.

figure 3 only needs three phases for operation: two phases (phase 1 and 2, $p_2=1$) for producing radial forces and one phase (phase 3, $p_1=2$) for producing torque by an armature alternating field. The radial force winding and the torque winding are composed of eight full pitch coils in all. This way there is a considerable reduction of the mechanical as well as the electrical expenditure.

Bearing force and torque can also be produced by using an arrangement of windings shown in figure 4. However the radial force currents and the torque currents are no longer decoupled. In this design the control of forces and torque takes place by superposition of the current components i_1, i_2 and i_3 in the current controllers. The determination of the coil currents i_I, i_{II}, i_{III} and i_{IV} follows from the equations listed in figure 3 and 4.

Figure 5 and 6 demonstrate, that depending on the current flow, it is possible to get a two-pole armature rotatory field as well as a four-pole armature alternating field. As a result of this combination the machine builds up torque as well as radial forces for stabilizing the rotor in two degrees of freedom.

The mechanical stresses built up at the stator surface

$$\sigma = \mathbf{T_m n} \tag{1}$$

can be calculated by the stress tensor $\mathbf{T_m}$ and the normal vector $\mathbf{n}$

$$\mathbf{T_m} = \begin{bmatrix} \mu H_x^2 - \frac{1}{2}\mu H^2 & \mu H_x H_y & \mu H_x H_z \\ \mu H_y H_x & \mu H_y^2 - \frac{1}{2}\mu H^2 & \mu H_y H_z \\ \mu H_z H_x & \mu H_z H_y & \mu H_z^2 - \frac{1}{2}\mu H^2 \end{bmatrix}. \tag{2}$$

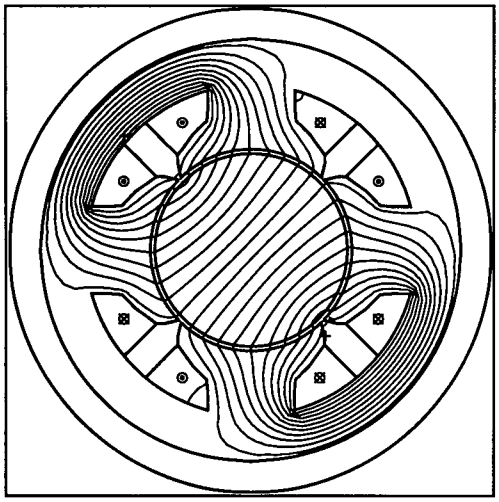

Fig. 5: Coil current configuration for creating a two-pole armature field.

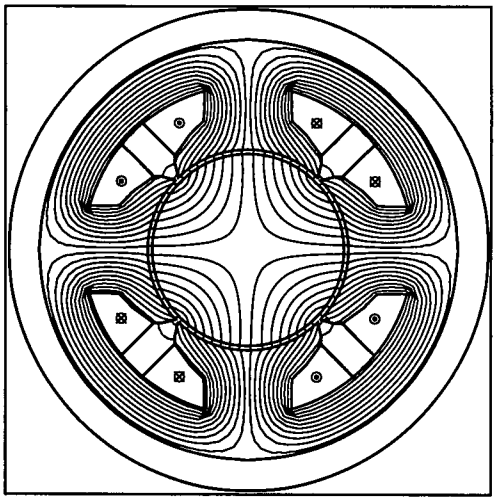

Fig. 6: Coil current configuration for creating a four-pole armature field.

On condition $\mu_{Fe} >> \mu_0$ and taking the winding currents into account by forming an infinitesimal thin current density distribution A on the stator surface, equation (1) can be simplified to

$$\sigma(\varphi) = \begin{bmatrix} \frac{B_n^2(\varphi)}{2\mu_0} \\ A(\varphi)B_n(\varphi) \\ 0 \end{bmatrix}. \tag{3}$$

where B_n denotes the normal component of the flux density.

The equations for forces and torque result in

$$\mathbf{F} = rl \int_0^{2\pi} \begin{bmatrix} \cos\varphi & -\sin\varphi & 0 \\ \sin\varphi & \cos\varphi & 0 \end{bmatrix} \begin{bmatrix} \frac{B_n^2}{2\mu_0} \\ AB_n \\ 0 \end{bmatrix} d\varphi \tag{4}$$

$$T = r^2 l \int_0^{2\pi} AB_n d\varphi. \tag{5}$$

The model for calculating the Maxwell forces and Lorentz forces as well as the torque is presented in figure 7. In comparison to the original motor design the model is slotless. The windings are substituted by concentrated current conductors at the stator surface.

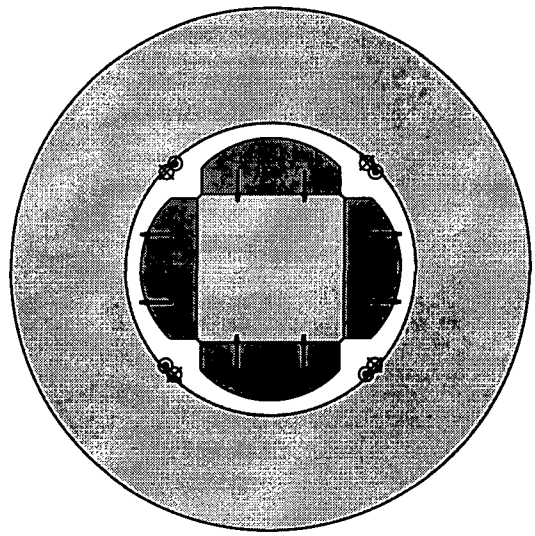

Fig. 7: Model for calculating Maxwell forces, Lorentz forces and torque.

The results of the calculations are shown in figure 8. The force vectors are determined for a constant current i_1 in phase 1 at different rotor positions. It can be noticed, that the Maxwell and Lorentz force vectors rotate in opposite directions. Thus the overall force is reduced in the flat region of the ellipse. Better results can be achieved with an exterior rotor design (Silber and Amrhein, 1998; Post, 1997) or by exchanging the pole pair numbers of motor and magnetic bearing components. However the latter leads to an increasing mechanical expenditure. The vector diagrams of phase 2 of the radial force winding are not displayed. They differ in an angular offset of 90°.

Nonlinear FE-computations of the original slotted design in figure 3 and 4 only yield insignificant differences to the calculations basing on the simplified linear model of figure 7. The resulting overall force vectors of FE- computations are shown in figure 9.

The elliptic locus curve of the force vector can be reproduced by two on circular curves in opposite direction rotating force vectors. This results in the following equations for the rotor-angle dependent radial forces of the windings 1 and 2

$$\mathbf{F_1} = (k_a e^{-j\delta} + k_b e^{j\delta}) i_1 \tag{6}$$

$$\mathbf{F_2} = (k_a e^{-j\delta} + k_b e^{j\delta}) i_2 e^{-j\frac{\pi}{2}} \tag{7}$$

and in trigonometric formulation

$$|\mathbf{F_1}| = k(\delta) i_1 \tag{8}$$

with

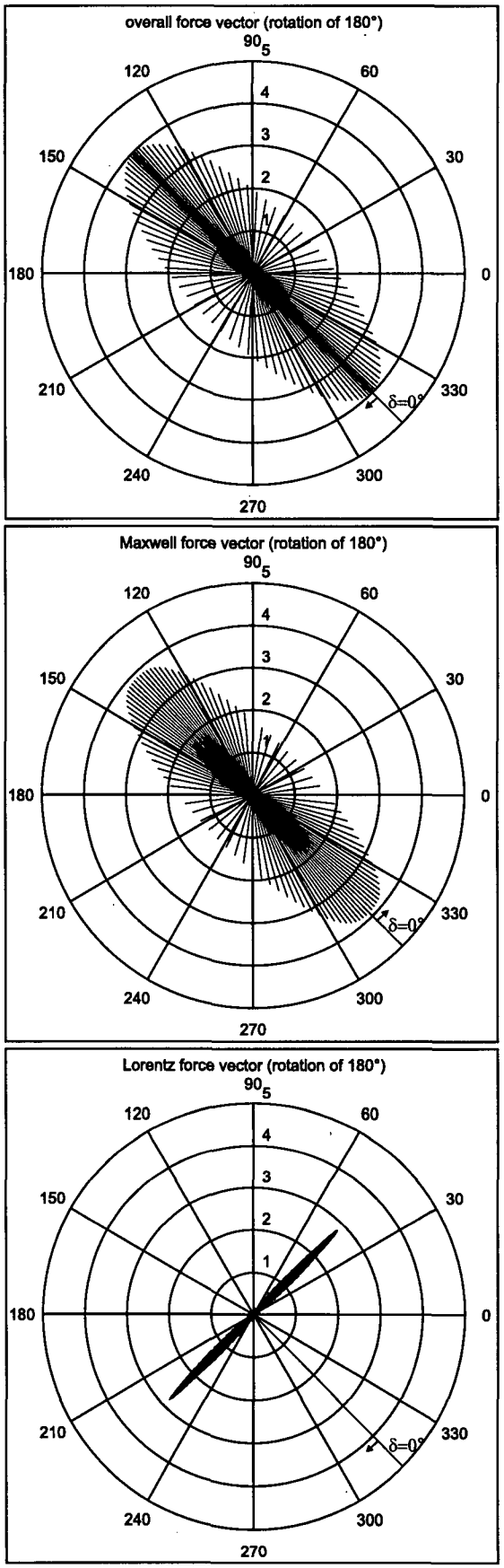

Fig. 8: Overall force, Maxwell force and Lorentz force vectors for different rotor positions δ (angular step: 2°) at constant phase current i_1.

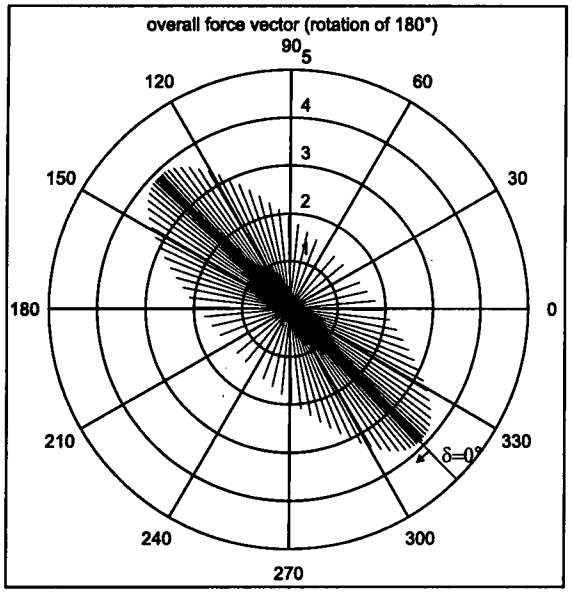

Fig. 9: Overall force vectors of nonlinear FE-computation at constant phase current i_1 (angular step: 2°).

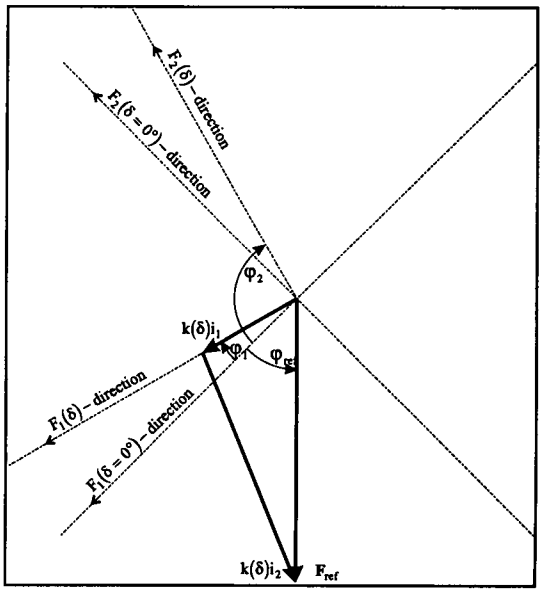

Fig. 10: Determination of the phase currents of the radial force winding.

$$k(\delta)=\sqrt{(k_a+k_b)^2\cos^2\delta+(k_b-k_a)^2\sin^2\delta} \tag{9}$$

$$\tan\varphi_1=\frac{k_b-k_a}{k_b+k_a}\tan\delta \tag{10}$$

The force F_2 is defined by

$$|\mathbf{F_2}| = k(\delta)i_2 \tag{11}$$

$$\varphi_2=\varphi_1-\frac{\pi}{2} \tag{12}$$

For an arbitrary force vector $\mathbf{F}_{ref}$ the corresponding phase currents can be calculated by the equations

$$i_{1ref}=|\mathbf{F}_{ref}|\frac{\cos(\varphi_{ref}-\varphi_1)}{k(\delta)} \tag{13}$$

$$i_{2ref}=-|\mathbf{F}_{ref}|\frac{\sin(\varphi_{ref}-\varphi_1)}{k(\delta)}. \tag{14}$$

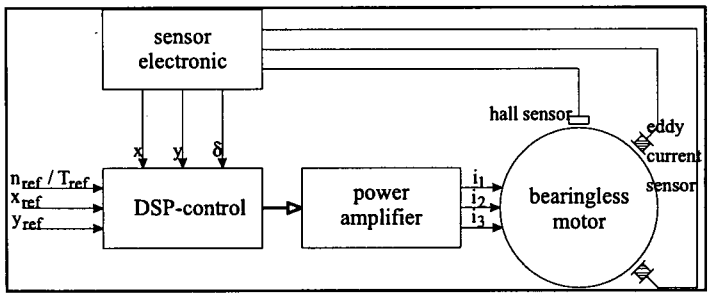

Fig. 11: Block diagram of the electronic.

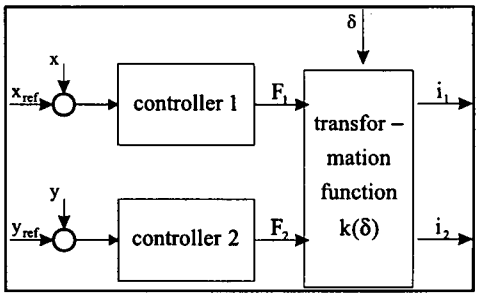

Fig. 12: Implementing the transformation function k(δ) (equ. (9)) into the control scheme.

The derivation of stator currents i_{1ref} and i_{2ref} is explained by the diagram of figure 10.
The average torque T_{ref} is impressed by the squarewave stator current i_3 and can be described as follows

$$i_{3ref} = \text{sign}(\sin\delta)\frac{T_{ref}}{k_{i_3}(\delta)}. \qquad (15)$$

The torque constant $k_{i_3}(\delta)$ can be determined by equation (5). Because of the sinusoidal flux linkage the torque curve is sinusoidal as well when the current is kept constant.

ELECTRONIC DESIGN

Figure 11 presents the electric circuit with a digital signal processor TMS 320C50 as central control unit in schematic form. Various control functions are implemented in the signal processor. This includes force and torque control, processing sensor signals or balancing the rotor by misalining rotation axis and principal axis of inertia. The acquisition of rotor position (fig. 11) is done by measuring the distance using eddy current sensors and measuring the rotor angle using hall sensors.

For the calculation of the actual current amplitudes from the force in tabular form stored functions are implemented to improve processing time. Figure 12 shows the corresponding part of the signal flow diagram using the transformation function of equation (9).

EXPERIMENTAL RESULTS

A first prototype of the bearingless single-phase motor with permanent magnet excitation has been built in interior-rotor design. Figure 13 shows the winding arrangement with four salient poles and the four-pole permanent magnet rotor inside a plastic slice. The sensors including the sensor electronics are below the motor. Radial position and speed control is performed by a TI TMS 320C50 signal processor.

The operation of the first prototype with sinusoidal flux density distribution shows good

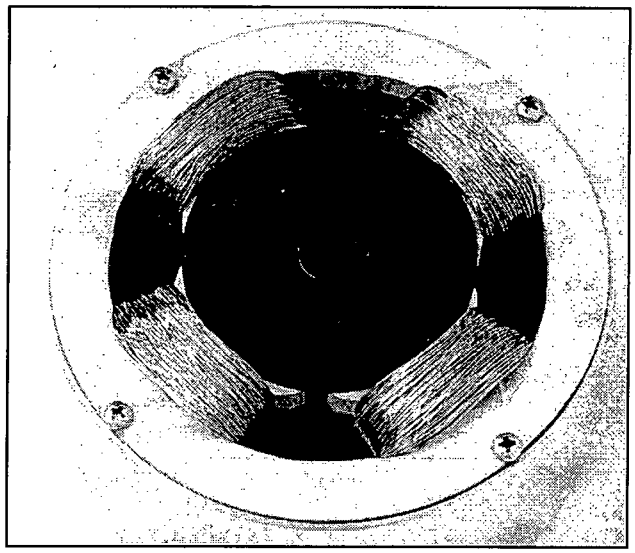

Fig. 13: Stator winding and permanent magnet rotor in interior-rotor design.

conformity with the technical spezifications. The measurements confirm the calculations done by analytical and FE-programs. As mentioned before the magnetic circuit has been designed for a sinusoidal air gap flux density distribution. Owing to the salient pole full pitch winding there must be a sinusoidal emf as well. Figure 14 shows that there is a good approximation. The torque characteristic shown in figure 15 is quite linear providing a good control performance. For the reason of the small axial length to diameter ratio no active axial position control is necessary for levitation. According to the application fields the bearingless motor has been tested at a nominal speed of 3000 rpm.

CONCLUSION

A new development of a bearingless single-phase brushless DC permanent magnet motor is presented. A two-phase winding system is integrated into the stator design of the motor offering the opportunity to produce radial forces for bearingless operation.

With the exception of the additional sensoric for rotor position measuring the presented motor/magnetic bearing system is comparable to a three-phase brushless AC permanent magnet drive in mechanical and electronical expenditure.

The presented bearingless single-phase motor with concentric full pitch windings is characterized by elliptical radial force locus curves. As a result of the noncircular locus curve a special transformation function $k(\delta)$ is necessary to derive the corresponding currents from the force components. Experimental tests with the first prototype show good results in motor and magnetic bearing performance.

Suitable application fields for the proposed bearingless motor are fluid pumps, vacuum pumps, fans or blowers with special requirements on speed range, lifetime, cleanness (chemical or medicine industry) or tightness.

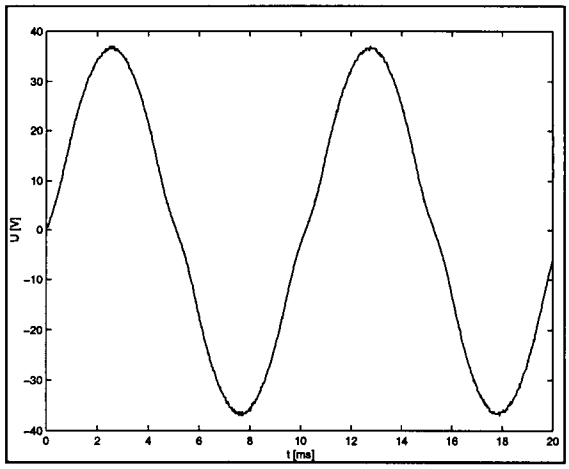

Fig. 14: Measured emf of the bearingless single-phase motor.

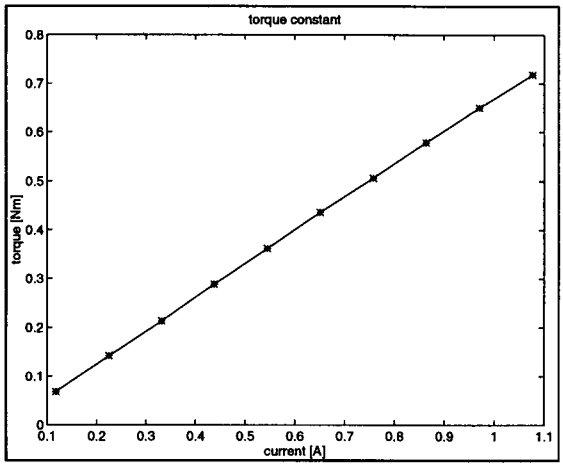

Fig. 15: Measured torque/current-characteristic of the bearingless single-phase motor.

ACKNOWLEDGEMENTS

The project was kindly supported by the Laboratory for Electrical Engineering Design (EEK) of Swiss Federal Institute of Technology, Zurich (ETH Zurich) and Sulzer Electronics AG, CH-Winterthur.

REFERENCES

Bichsel, J. 1990. „Beiträge zum lagerlosen Elektromotor", Dissertation, ETH Zürich.

Bleuler, H., H. Kawakstsu, W. Tang, W. Hsieh, D. K. Miu, Y. Tai, F. Moesner and M. Rohner. 1994. „Micromachined active magnetic bearings", Proc. 4th Int. Symp. Magn. Bearings, Zurich, Switzerland: 349-352.

Chiba, A. and T. Fukao. 1994. „The maximum radial force of induction machine type bearingless motor using finite element analysis", Proc. 4th Int. Symp. Magn. Bearings, Zurich, Switzerland: 333-338.

Herzog, R. 1991. „Ein Beitrag zur Regelung von magnetgelagerten Systemen mittels positiv reeller Funktionen und H^{∞} - Optimierung", Dissertation, ETH Zürich.

Ohishi, T., Y. Okada and K. Dejima.1994. „Analysis and design of a concentrated wound stator for synchronous-type levitated motor", Proc. 4th Int. Symp. Magn. Bearings, Zurich, Switzerland: 201-206.

Oshima, M., S. Miyazawa, T. Deido, A. Chiba, F. Nakamura and T. Fukao. 1996. „Characteristics of a permanent magnet type bearingless motor", IEEE Trans. Ind. Appl., Vol. 32, No.2: 363-369.

Post, C. 1997. „Konstruktion eines lagerlosen Einphasenmotors", Diplomarbeit, Johannes Kepler Universität Linz.

Schöb, R. 1993. „Beiträge zur lagerlosen Asynchronmaschine", Dissertation, ETH Zürich, 1993.

Schöb, R. and N. Barletta. 1996. „Principle and application of a bearingless slice motor", Proc. 5th Int. Symp. Magn. Bearings, Kanazawa, Japan: 313-318.

Schöb, R. and J. Bichsel. 1994. „Vector control of the bearingless motor", Proc. 4th Int. Symp. Magn. Bearings, Zurich, Switzerland: 327-332.

Silber, S. and W. Amrhein. 1998. „Design of a Bearingless Single-Phase Motor", Proc. PCIM, vol. Intelligent Motion.